UNIVERSITEIT•STELLENBOSCH•UNIVERSITY
jou kennisvennoot • your knowledge partner

Stochastic inversion of fire test data for the T-dependant thermal diffusivity of SA pine

by

Liza Stewart
21555575

Project(Civil Engineering)458

Final Draft

Study leader: Prof N de Koker

October 2021

Declaration

Ek, die ondergetekende, verklaar hiermee dat die werk in hierdie verslag vervat, my eie oorspronklike werk is.

Signature: .....
L. Stewart

Datum: .....

PROJECT (CIVIL ENGINEERING) 458: SUMMARY

Student: L. Stewart
Medewerker:

Title of Project
The Stochastic inversion of fire test data for the T-dependant thermal diffusivity of SA pine
Goal
To determine the probability distribution of thermal diffusivity of SA-pine, using statistical inversion theory and Markov Chain Monte-Carlo as.
What did I do that was unique
What are my findings?
Usefulness of results?
In geval meer as een student, welke deel het jy gedoen?
N.V.T.
What aspects of the project will be further explored after the project has ended?
What are the expected benefits of further research?
What plans are being made for further research?

Student Date Lecturer

Abstract

In this report stochastic inversion methods such as Markov Chain Monte-Carlo and optimisation methods were used to determine the thermal diffusivity of SA-Pine. A finite element model was constructed to model a 100mm element exposed to the ISO 846 Fire curve. This model was used within the likelihood function of New κ-values were found from MCMC and MAP analysis. The MCMC and MAP $|kappa$-values were not equal which supports the hypothesis that the distribution is not normal. The FEM model using the new κ-values was closer to the measured temperatures.

Contents

List of Figures

Nomenclature

Constants

g =	$9.81\,\mathrm{m/s^2}$	

Variables

κ	Thermal conductivity	$[\,\mathrm{W/m{\cdot}K}\,]$
α	Thermal diffusivity	$[\,\mathrm{m^2/s}\,]$
c_ρ	Heat capacity	$[\,\mathrm{J/kg/K}\,]$

Chapter 1

Introduction

This chapter will introduce the problem addressed in this project. Previous similar projects as well as the value of this research will also be addressed.

1.1 Background and Motivation

Traditionally the thermal conductivity, otherwise referred to as the κ-value, of timber is based simply on the EN 1995:1-1-2004 or similar standards. This research project will aim to obtain the thermal diffusivity of cross-laminated SA-Pine timber by further analysing data obtained by S. van der Westhuyzen for his study of the samples' charring rate.

The thermal diffusivity of timber is an unobservable quantity that cannot be measured directly. Instead, it is related to measurements of temperature and time through differential models. When heat diffusion is calculated using Finite Element methods(TODO: choose which FEM), the process is usually simplified to a linear problem (Fish, 2007). Due to the changes in thermal diffusivity of timber with temperature, as can be seen in EN 1995:1-1-2004(pg number T) and Figure 3.21, the diffusivity cannot be linearly modelled. Therefore, the problem lends itself to being analysed by inversion techniques. The aforementioned approach will allow us to obtain information about the diffusivity based on the combination of the information assumed prior to measuring, further referred to as the prior, and the measured data. Using statistical inversion leads to a probability distribution that provides us with a collection of diffusivity estimates and their corresponding probabilities. The approach taken in this report is unique due to the nature of data used. As the main purpose of this data was not to obtain thermal conductivity but to determine char rates. The difference in purpose means that more assumptions had to be made in contrast to a experiment that intended to determine the thermal conductivity and would have controlled those variables.

Currently, the fire rating of specific timber samples is based on fire tests

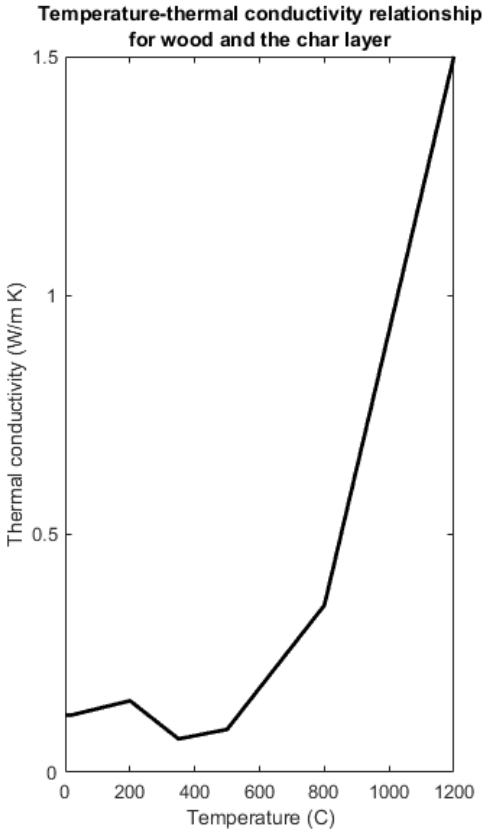

Figure 1.1: Standard temperature-thermal conductivity relationship for timber from (CEN, 2004)

conducted in a furnace. The furnace is kept at increasing temperatures corresponding with the Standard or ISO 834 fire curve as specified in ISO 834 ISO (1999). This process becomes very costly if it has to be repeated every time that timber is used for construction, as timber usage for multiple story construction projects has increased over the past decades. This increase is partially due to the sustainability of timber as a construction material: not only is it renewable but it also has a small carbon footprint (Salvadori, 2017). Obtaining and standardising different thermal diffusivity values for different species of timber will assist in more accurate modelling. If modelling accuracy can be increased, the option to use modelling as either confirmation of fire tests or instead of small scale fire tests will become more feasible.

/

1.2 Aim and objectives

During the course of the project, the student will aim to meet the following objectives:

1. Modify a Finite Element Model into an accurate and effective function;
2. Compare the model data to the actual acquired data;
3. Solve for the thermal diffusivity using Bayes' theorem of inverse problems; and
4. Evaluate and explore the posterior probability distribution using the following methods:
   (a) Maximum a Posteriori
   (b) Markov-Chain Monte Carlo

1.3 Literature study

In their article *Simple Method to Determine the Diffusivity of Green Wood*, Frayssinhes *et al.* determine the global diffusivity of a Douglas fir green log using inverse identification methods. Their experiment was set up by immersing the log with K-type thermocouples into a boiler filled with water at 60°C. These K-type thermocouples were very specifically placed to improve the accuracy of the diffusivity ratio calculation. The finite element model constructed for their calculations used linear interpolation with four-node quadrangle elements. An analytical model was also constructed using the heat propagation equation(TODO?heat diffusion?). This research intended to assist the peeling industry in making the pretreatment process more cost-effective. The method proved to be effective at determining the thermal diffusivity of green Douglas fir logs, as the κ-values obtained were comparable to those from literature. The methods used by Frayssinhes *et al.* (2020) are similar to the methods described later in the report. A crucial difference remains as the temperatures at which these experiments were conducted as well as the final usage of the data differ greatly.

Wagner *et al.* wrote an article in March 2021 where Bayesian model inversion was used with stochastic spectral embedding. Spectral embedding or spectral likelihood expansion is used to solve for the likelihood function in such a way that sampling is not necessary. The relevance of the research done by Wagner *et al.* to this report is in the creation of the bayesian model to solve a heat diffusion problem.

Chapter 2

Technical Foundation

In this chapter, the detailed explanations of algorithms and concepts applied throughout the project are presented. the purpose of this chapter is to enable the reader to better understand the implementation and reasoning for the usage of specific methods.

2.1 Thermal properties of timber

Specific thermal properties of timber need to be thoroughly understood to allow for accurate modelling interpretation of the results. After 100 °C, the temperature exposure causes the breakdown of the timber structure in such a way that the structure will not return to the same state after cooling. This breakdown is generally referred to as thermal degradation. The degradation can be broken into four categories (White and Dietenberger, 2001) (Shi and Chew, 2021). These four categories are based on the different reactions that take place and are briefly summarised below. Above 100 °C and below 200 °C, the moisture in the timber is evaporated and other non-combustible gasses are released. Between 200 °C and 300°C, carbon-monoxide is released in significant quantities and some of the timber components undergo a change in chemical composition due to the high temperatures. Temperatures after 300 °C and before 450 °C are significant due to the amount of flammable volatiles released and the break of carbon linkages at 370 °C. At temperatures higher than 450 °C the remaining timber is char and any further degradation is due to oxidation from carbon-monoxide, - dioxide and water. These phases should be clear in the results and data. (TODO add lines for phases)

All the thermal properties of various timber species at high temperatures were discussed in a research article by Shi and Chew (2021). In their article, they provide a general expression for the thermal conductivity of softwoods (Equation 2.1) and char (Equation 2.2).

$$\alpha = 0.124 + 0.8432 \times 10^{-4}(\mathrm{T} - 293) \tag{2.1}$$

$$\alpha = 0.091 + 8.2 \times 10^{-4}\mathrm{T} \tag{2.2}$$

For this project, the temperature of char will be used as 300 °C following the research of van der Westhuyzen *et al.*. Using the equations in by Shi and Chew the following κ-values (Equation 2.3) are obtained.

$$\mu = \begin{bmatrix} 0.0993 \\ 0.1044 \\ 0.1077 \\ 0.1111 \\ 0.1162 \\ 0.3780 \\ 0.5010 \\ 0.7470 \\ 1.0750 \end{bmatrix} \begin{matrix} 0\ ^\circ\mathrm{C} \\ 60\ ^\circ\mathrm{C} \\ 100\ ^\circ\mathrm{C} \\ 140\ ^\circ\mathrm{C} \\ 200\ ^\circ\mathrm{C} \\ 350\ ^\circ\mathrm{C} \\ 500\ ^\circ\mathrm{C} \\ 800\ ^\circ\mathrm{C} \\ 1200\ ^\circ\mathrm{C} \end{matrix} \tag{2.3}$$

From the big difference between these values and the Euro code values, it is clear that these simple equations are not sufficient for determining the thermal conductivity of pine.

2.2 Finite Element Method

Finite element methods (or finite element analysis) is used when the behaviour of an element cannot be accurately depicted by a simple mathematical equation.

2.2.1 Origin

The finite element method (FEM) used today is the sum of decades of research. In an article by Gupta and Meek, they discuss the five main contributors to the finite element method. According to Gupta and Meek (1996) the idea behind the finite element method was initially explored in the 1943 article by Courant. Courant acknowledges the complex nature of mathematical problems in his first paragraph by stating: "Mathematics is an indivisible organism uniting theoretical contemplation and active application." He goes on to discuss the variational method created by (Ryes?)

2.2.2 Concept

A larger element is broken into smaller elements. Assumptions made on a smaller scale have a lesser effect on the final answer than the same assumptions

made on a large scale would have had. Therefore choosing more elements leads to a more accurate model.

2.2.3 Boundaries

An important part of how finite element models are how the known information is embedded into the model. The main way this is done is by defining boundary conditions at known points. The two types of boundary conditions used in this project are Dirichlet boundaries and Newmann boundaries.

Named after Johann P.G.L Dirichlet (Cheng and Cheng, 2005), Dirichlet boundaries force the solution function to be equal to the prescribed value at the boundary. Newmann boundaries prescribe that the derivative of the solution function be equal to the predetermined value. In the context of this problem, the Dirichlet boundaries prescribe the temperatures at the boundaries and the Newmann boundaries prescribe the heat flux at the boundaries.

2.2.4 Heat diffusion

In its simplest form, the one-dimensional heat diffusion equation is a partial differential equation 2.4 dependant on the temperature and thickness of the element. The heat diffusion equation is based on Fourier's Law

$$q = -k\frac{dT}{dx} = -ku_{,x} \tag{2.4}$$

2.2.5 Heat conduction

TODO: - Explain Galerkin Weak form

2.3 Bayes' theorem of inverse problems

The method of statistical inversion is dependant on a fundamental understanding of the Bayes' theorem of inverse problems. The student obtained this understanding through studying Chapter 3 of statistical and Computational Inverse problems by Kaipio and Somersalo (2005), further referred to merely as Kaipio. There are four principles of Statistical inversion that is essential to the thorough understanding of these models. Firstly, it is the principle that any variable in the model needs to be modelled as a random variable. This randomness is based on the extent of information that is available. To ensure that the extent of knowledge is accurately portrayed in the model, the extent of knowledge will be coded into the probability distributions assigned to the different variables. Finally, it needs to be understood that the solution

of a statistical inversion is a posterior probability distribution. A generalized equation of Bayes' theorem can be seen in 2.5 taken from Kaipio.

$$\pi_{\text{post}}(x) = \pi(x|y_{\text{observed}}) = \frac{\pi_{\text{pr}}(x)\pi(y_{\text{observed}}|x)}{\pi(y_{\text{observed}})} \tag{2.5}$$

2.4 Markov Chain Monte Carlo

Markov Chain Monte Carlo (MCMC) is a method of integration that will be used to determine the mean of the κ-values at specific temperatures. Markov Chain Monte Carlo is a method that was created by combining the concept of Monte Carlo sampling and a Markov Chain. To fully understand MCMC, its underlying methods must be investigated further. For a better understanding of this concept, *Introducing Markov chain Monte Carlo* by Gilks *et al.*, Kaipio, and various websites (Brownlee, 2019), (Wiecki, 2015) were consulted.(RIJK: is sin lomp?)

2.4.1 Markov Chains

The core principle of a Markov chain is that the next value (x_{n+1}) in a sequence is dependent on the current value(x_n). A step size that indicates the range within the next point falls in. Values are then randomly generated but restricted to be within this range. This concept can be visualised as follows: the accepted point (x_1) is in the centre of a cube. The next possible random point is randomly generated but still within the cube(our search range). After this next number is selected, the cube moves such that the new point(x_2) is now the centre, and so it continues. See Figure 2.1 for clarification. The above example simplifies the concept, but this understanding can now be expanded. If every coordinate direction in the aforementioned simple example is seen as a single entry in the x vector, then the example has three independent values. More or fewer values can be used depending on the problem. Another level of complication can be added if it is taken into account that every point in the cube is no longer equally likely. A distribution within the cube can be chosen, for example simply a normal distribution The shape of the cube then warps into a stranger shape with points closer to the center being more likely choices and the edges being less likely.

The purpose of a Markov Chain is for the chain to converge to a distribution and be independent on the very initial estimation. In principle, it should then reach a near stationary distribution. Since Markov Chains are not used if we know the answer, a way to determine when values are no longer affected by the initial estimate is needed Gilks *et al.* (1996). The simple proposed solution is the concept of burn-in. The concept of conventional burn-in for usage in Markov Chains are disputed as the Markov Chain itself is created in such a way

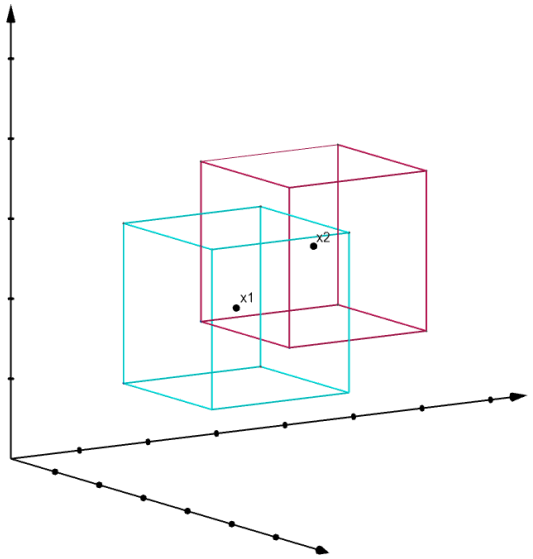

Figure 2.1: Three-dimensional example of Markov Chain application (Created on `https://www.geogebra.org/3d`)

that values are only directly dependent on the value immediately before them Meyn and Tweedie (1993). Burn-in in the Markov Chain sense can simply be referred to as the removal of the initial samples of low probability to increase the accuracy of the average taken after all the iterations Cook (2016).

2.4.2 Monte Carlo Integration

Monte Carlo integration is used to evaluate a probability distribution that cannot be solved simply. The evaluation is done by drawing a collection of random values from the distribution. These values are then used as the sample, and a sample mean is taken. The arithmetic sample mean can be used to approximate the population mean per the law of large numbers (Gilks *et al.*, 1996).

2.4.3 Metropolis-Hastings Algorithm

The Metropolis-Hastings algorithm is one of the available simulation methods based on the MCMC principles. For this project, the Metropolis-Hastings algorithm was chosen above the Gibbs-sampler TODO

All of the random samples generated by the Monte Carlo integration can not be immediately accepted. Here, the acceptance criterion comes into play. There are multiple options for how a posterior is deemed acceptable; these are elaborated on in the book *Monte Carlo Statistical Methods* by Robert and

Casella. The most general acceptance criterion is set out in Equation 2.6 and comes from Kaipio.

$$\begin{aligned} &\text{if} \quad \frac{\pi(x_2)}{\pi(x_1)} > 1 \quad \text{Accept automatically} \\ &\text{or} \quad \frac{\pi(x_2)}{\pi(x_1)} > \text{rand} \quad \text{Accept} \\ &\text{else reject and reselect } x_2 \end{aligned} \tag{2.6}$$

2.5 Maximum a Posteriori

To ensure a thorough investigation of the thermal diffusivity of timber the posteriori function will also be optimised to obtain the value with the highest probability, maximum a posteriori, in addition to the mean. As the implementation will be done using built-in optimisation functions in Matlab the technical aspects will briefly explain how that function works. The function used is `fminsearch.m`. In the name of the function, it can be seen that the function will be minimised. This seems counter-intuitive since the intention is to find the maximum of the function. Luckily the minimum is simply a negative maximum.

According to the `fminsearch` Matlab documentation (`https://ch.mathworks.com/help/matlab/ref/fminsearch.html`) , the algorithm is based on the Nelder-Mead algorithm (Lagarias *et al.*, 1998). The Nelder-Mead algorithm is an unconstrained heuristic direct search method. The heuristic aspect of the algorithm means that it searches the function space in a guided random manner.

Nelder-Mead uses a simplex, a triangle in the dimension needed, to find the minimum. In two-dimension, the simplex is simply a triangle, where each point has a x and y coordinate and is notated as. A starting value needs to be provided to the algorithm, this will then be one of the points in the first simplex. All the points on the simplex are ordered from best to worst, where the smallest value ($f(x)$) is best if minimising. In the two-dimensional example, the centroid of the two best points (x_l, x_s) are calculated, from there using the value of the function at the simplexes and the centroid transformations can be performed to find even smaller values. The transformations are applied to change the worst point (x_h) until it is no longer the worst.

The transformations are performed in a specific order. The first transformation is reflection. Point x_h is mirrored around the line that passes through the centroid and x_l and x_s to create x_r. The idea behind this is that the values are lower in that direction so the algorithm attempts to take the biggest stride possible to a lower value. If x_r is better than x_r the triangle is expanded and x_e is even further in the assumed minimising direction. If x_r is not better than

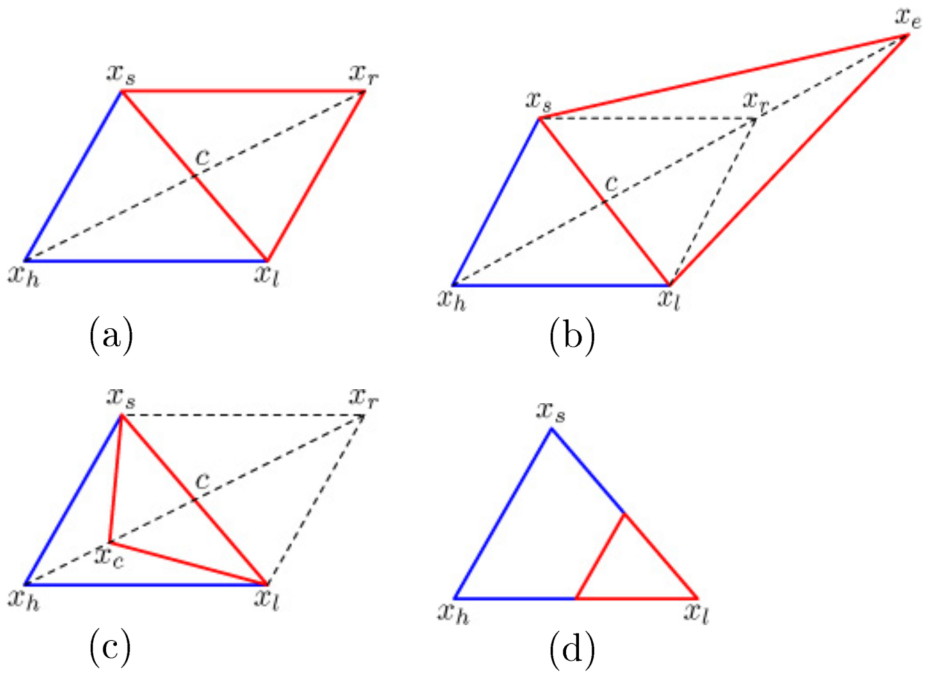

Figure 2.2: Visual representation of Nedler-Mead transformations a) Reflection, b) Expansion, c) Contraction, d) Shrink contraction (Source:`https://codesachin.wordpress.com/2016/01/16/nelder-mead-optimization/`)

x_h, the reflected point is rejected and the original x_3 is contracted closer to x_1 and x_2. This contracted point (x_c) should ideally have a smaller value than x_h, if not a shrink contraction needs to be performed. In a shrink contraction, x_h and x_s are redefined and pulled closer to x_l with hopes of finding the minimum near the best point.

The result is a simplex that moves over a surface in search of the lowest point and as it reaches that point it shrinks until all the points are practically at the same place. When this happens or the points are close enough to each other as defined when initializing the code the algorithm stops. Below in Figure 2.5, the different transformations can be seen.

Chapter 3

Implementation

This chapter will elaborate on the test data used as well as the process that was followed to achieve the results in Chapter 4.

3.1 Existing data

The data used was acquired by van der Westhuyzen *et al.* (2020) for an article assessing the charring rate of both SA-Pine and Eucalyptus. For the purpose of this project, only the data obtained from the SA-Pine test was considered and analysed.

3.1.1 Summary of test

The test was conducted on a sample panel of 100 mm by 0.9 m $\times$0.9 m cross-laminated SA-pine. This sample was then divided into nine cubes of 100 mm $\times$100 mm $\times$100 mm. Each cube was fitted with seven Type K-thermocouples placed at consecutive 16.5 mm drilled holes, as can be seen in Figure 3.1. The test panel was tested in a furnace and was exposed to the standard ISO 834 Fire curve 3.2 on one side and room temperature on the other. The panel was exposed to the fire curve for 50 minutes, at which stage near complete de-lamination was observed and the test ended.

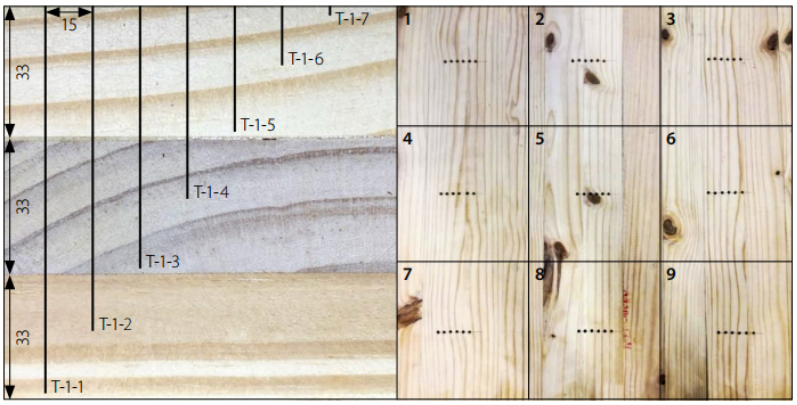

Figure 3.1: Thermocouple layout in test conducted by van der Westhuyzen *et al.* (2020) cross-section (left) and overall layout (right)

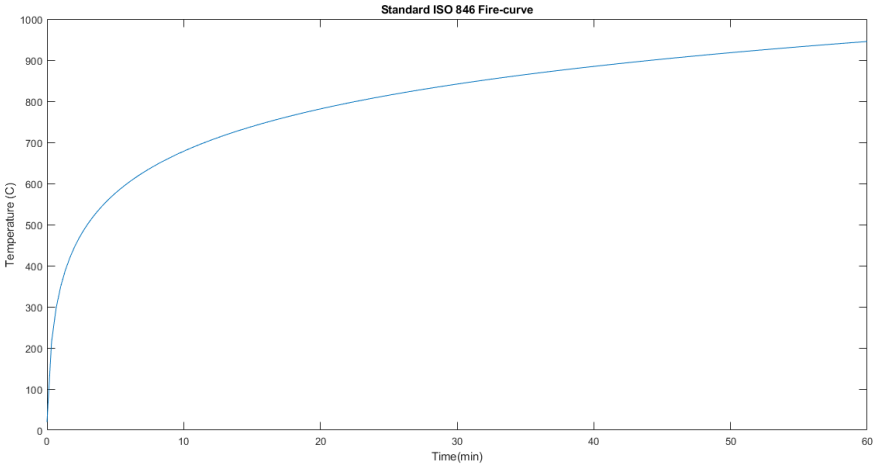

Figure 3.2: Standard ISO fire curve TODO

In Figure 3.1.1

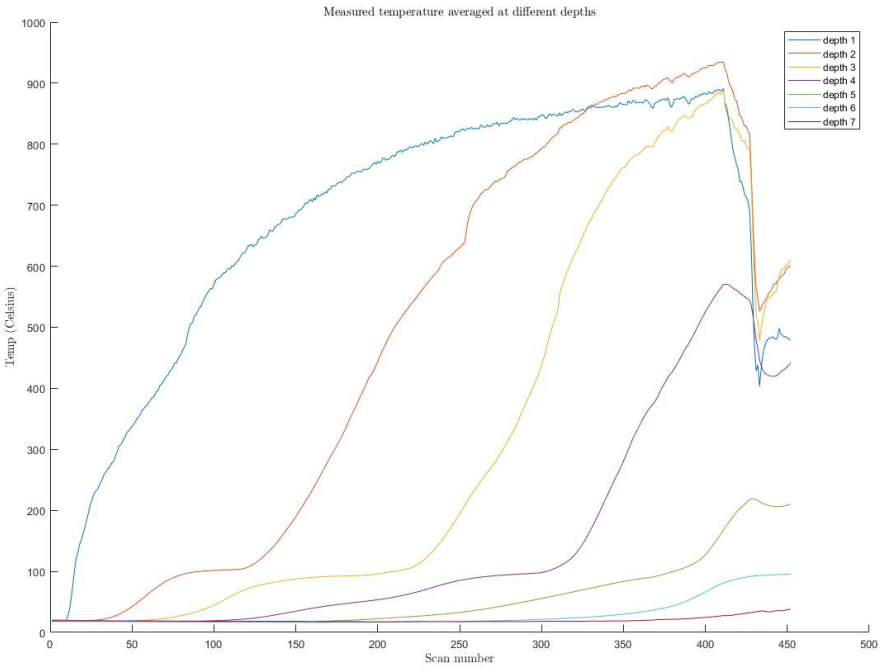

3.1.2 Potential inaccuracies

As with most tests, everything is not always perfect. The potential inaccuracies are discussed below. In the data, it was observed that two of the thermocouples broke during testing; this resulted in temperature with a magnitude of 10^{13}. Such a temperature is impossible, as the highest ever recorded temperature reached was 4×10^{12} and that only occurred in a atomic explosion. This malfunction required that two of the depth measurements were no longer the average between nine samples but instead the average between eight. Another inaccuracy that could potentially influence the accuracy of the final result is the accuracy of the depth of the holes in which the thermocouples were placed.

There is also debate about the significance of the contribution of the timber burning to the temperature inside the furnace. For the purposes of this project, it will be assumed that the timber burning does not contribute to the temperature inside the furnace.

3.2 Finite Element Modelling

A one-dimensional finite element model that simulates what we expect to obtain from the fire tests based on the simplified κ-values provided in EN 1995:1-2-2004 is modified into a function. This function should provide the

temperature of the modelled element based on a specified location and thermal conductivity. The derivation and adaptation of the model are expanded on below.

3.2.1 Derivation

Assumptions were made to simplify the model, they were as follows

1. The air on the side of fire follows the temperature of the fire curve.
2. The air on the cold side remains at 20°C.

Stationary heat conduction

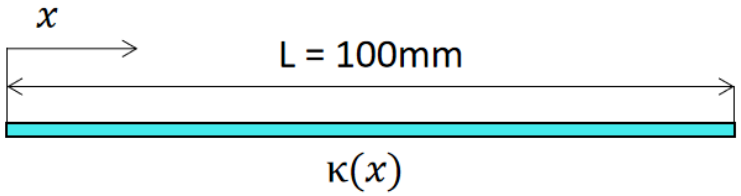

Figure 3.3: Visualisation of element that is modelled in one-dimension

The derivation started as a one-dimensional stationary heat conduction problem with the below equations as a starting point.

$$q_{,x} - f = 0 \ ...(1) \qquad q = -\kappa u_{,x} \ ...(2) \tag{3.1}$$

Integrating Equation 3.1 (1) over the length of the element(shown in Figure 3.2.1) and introducing a weighting function $w(x)$ we obtain 3.2. Since the derivative of $w(0)$ is known and $q_{,x}$ is unknown. The first term in 3.2 is integrated by parts. After the integration by parts and substituting q with 3.1 (2), Equation 3.3 is created.

$$\int_{x=0}^{L} w q_{,x} dx - \int_{x=0}^{L} w f dx = 0 \tag{3.2}$$

$$\int_{x=0}^{L} w k u_{,x} dx + \int_{x=0}^{L} w f dx - w q|_0^L = 0 \tag{3.3}$$

In Equation 3.3 the u and w need to be defined. Assuming $u \approx u^h$ and $w \approx w^h$ and using the basis function (N^A), Equation 3.4 is obtained.

$$\begin{aligned} u_e^h &= \sum_B N^B d^B \quad ; \quad w_e^h = \sum_A N^A c^A \\ u_{e,x}^h &= \sum_B N_{,x}^B d^B \quad ; \quad w_{e,x}^h = \sum_A N_{,x}^A c^A \end{aligned} \tag{3.4}$$

Substituting the u and w functions back, we obtain the Galerkin weak form shown in Equation 3.5. In Equation3.5 the A_N refers to the nodes that have Newmann boundaries(TODO explained in 2.2). The variables c^A and d^B are independent of x and can therefore be taken out of the integral. The sum over A and B are also taken out of the integral. After the summing is applied a matrix of all the possible combinations between A and B can be used to replace the sum. The resulting matrices are shown in Equation 3.6. When written in matrix form the summing is implied, if matrix form is not written then the expression referrers to the terms that will still be summed.

$$\begin{aligned} \sum_e \int_{\Omega_e} w_{e,x}^h k u_{e,x}^h dx + \sum_e \int_{\Omega_e} w_e^h f dx - w(L) q_L + w(0) q_0 &= 0 \\ \int_{\Omega_e} \sum_A \sum_B N_{,x}^A c^A k N_{,x}^B d^B dx + \int_{\Omega_e} \sum_A N^A c^A f dx - \sum_{A \in A_N} c^A q^A &= 0 \end{aligned} \tag{3.5}$$

$$\mathbf{c}_e^T \mathbf{K}_e^{AB} \mathbf{d}_e + \mathbf{c}_e^T \mathbf{F}_e^f - \mathbf{c}_e^T \mathbf{F}_e^q \tag{3.6}$$

where

$$\begin{aligned} K_e^{AB} &= \int_{\Omega_e} N_{,x}^A N_{,x}^B k dx \\ F_e^{Af} &= \int_{\Omega_e} N_{,x}^A f dx \\ F_e^{Aq} &= \begin{cases} q(x_N) & \text{for } x \in \Gamma_N \\ 0 & \text{for other} \end{cases} \end{aligned}$$

Boundaries

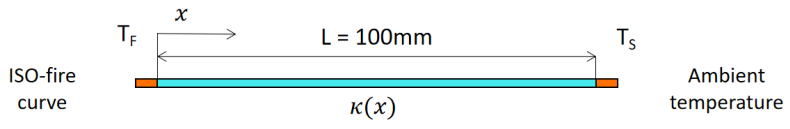

Figure 3.4: Visualisation of one-dimensional element with air elements and external conditions added

One of the additional difficulties in modelling is that the known boundary temperatures are measured in the air of the furnace and assumed for the air outside the furnace. Initially, a long element of air was modelled. This element is then overlaid with the timber element to effectively add an air element it each end of the timber element as depicted in 3.2.1 In the air elements, both heat convection and heat radiation need to be taken into account. The equations for heat convection and radiation can be seen in Equation 3.7 and 3.8.

$$\begin{aligned} q_{\text{adv}} &= \nu\rho c_p \Delta T \quad = \quad h\Delta T \\ \nu &= \text{velocity m/s} \\ \rho &= \text{density of air} \\ c_\rho &= \text{heat capacity of air} \end{aligned} \tag{3.7}$$

$$\begin{aligned} q_{\text{rad}} &= \varepsilon\sigma\phi\left(T_f^4 - T_S^4\right) \\ \varepsilon &= \text{emissivity} \\ \sigma &= \text{Stefan-Boltzmann} \\ & \quad 5.670e^{-}8[W/(m^2K^4)] \\ \phi &= \text{view factor; } 1 \quad \text{here} \end{aligned} \tag{3.8}$$

Given that T_S and T_F are known a new equivalent heat flux value can be calculated as in Equation 3.9.

$$q_{\text{con}}^{\text{equiv}} = \kappa^{\text{equiv}} \frac{\Delta T}{\Delta L} = q_{\text{rad}} + q_{\text{adv}} \tag{3.9}$$

Due to the clear relationship between heat flux and thermal diffusivity the equivalent diffusivity(κ^{equiv}) can be calculated as shown below in Equation 3.10.

$$\begin{aligned} \kappa^{\text{equiv}} &= \frac{[q_{\text{rad}} + q_{\text{adv}}]}{\Delta T} \\ &= \frac{\epsilon\sigma\phi\Delta\left(T^4\right)}{\Delta T/\Delta L} + h\Delta L \\ &= \frac{\epsilon\sigma\Delta\left(T^4\right)}{\Delta T} + h \end{aligned} \tag{3.10}$$

One-dimensional diffusion

The concept of diffusion is thoroughly explained in 2.2(TODO) below the mathematical application is explained and steps that were taken to obtain the final model is shown.

$$q_{,x} - f = \frac{\partial Q}{\partial t} = c_p \frac{\partial u}{\partial t} \quad ...(1) \qquad q = -\kappa \frac{\partial u}{\partial x} \quad ...(2) \tag{3.11}$$

Substituting Equation 3.11(2) into 3.11 and taking the derivative as indicated $(q_{,x})$ gives Equation 3.12. As previously disccussed heat conduction (α) is heat diffusion (κ) divided by specific heat (c_p).

$$\begin{aligned} \therefore -\kappa\frac{\partial^2 u}{\partial x^2} - f = c_p\frac{\partial u}{\partial t} \rightarrow f = 0: \\ \frac{\partial^2 u}{\partial x^2} = -\frac{c_\rho}{\kappa}\frac{\partial u}{\partial t} \\ \text{or} \\ \frac{\partial u}{\partial t} = -\alpha\frac{\partial^2 u}{\partial x^2} \end{aligned} \tag{3.12}$$

Let $c_p = \lambda$

$$\therefore -\kappa u_{,xx} - \lambda u_{,t} = f \tag{3.13}$$

Then:

$$\int_0^L w q_{,x}\mathrm{d}x - \int_0^L w\lambda u_{,t}\mathrm{d}x - \int_0^L w f\mathrm{d}x = 0 \tag{3.14}$$

Similar to what was done in 3.4 a special approximation is made to obtain Equation 3.15.

$$u \approx u^h \rightarrow u_e^h = \sum_A N^A d^A \quad ; \quad w_e^h = \sum_A N^A L^A \tag{3.15}$$

$$\rightarrow \sum_e \int_{\Omega^e} w_{e,x}^h \kappa u_{e,x}^h \mathrm{d}x_e + \sum_e \int_{\Omega^e} w_e^h \lambda u_{e,t}^h \mathrm{d}x_e + \sum_e \int_{\Omega^e} w_e^h f \mathrm{d}x_e - \sum_{e\in\epsilon_A} w q_N = 0 \tag{3.16}$$

$$*_1 : \int_{\Omega^e} \sum_A \sum_B N_{,x}^A c^A \kappa N_{,x}^B d^B \mathrm{d}x = \sum_A \sum_B \left[\int N_{,x}^A N_{,x}^B \kappa \mathrm{d}x\right] d^B = \mathbf{c}_e^T \boldsymbol{\kappa}_e \mathbf{d}_e$$

$$*_2 : \int_{\Omega_e} \sum_A \sum_B N^A c^A \lambda N^B \dot{d}^B \mathrm{d}x = \sum\sum c^A \left[\int N^A N^B \lambda \mathrm{d}x\right] d^B = \mathbf{c}_e^T \mathbf{M}_e \dot{\mathbf{d}}_e$$

$$*_3 : \int_{\Omega^e} \sum_A N^A c^A f \mathrm{d}x = \sum c \int_B^A N f \mathrm{d}x = \mathbf{c}_e^T \mathbf{F}_e^B$$

$$*_4 : \sum_{A\in\mathcal{A}} \kappa^A q_N^A = \mathbf{c}_e^T \mathbf{F}_e^q$$

From all the above equations the below matrix formulation could be assembled:

$$\mathbf{c}^T\boldsymbol{\kappa}\mathbf{d} + \mathbf{c}^T\mathbf{M}\dot{\mathbf{d}} = \mathbf{c}^T\mathbf{F} \tag{3.17}$$

Solving:(TODO: date 15/10 last)

3.2.2 Existing Model

For this project, an existing finite element model of heat diffusion by Prof. N de Koker was modified for usage in the Bayes' theorem 2.5. This model is used to determine the likelihood function. The current model uses the standard Euro code κ-values as well as the specific heat specified in the (CEN, 2004) shown in Equation 3.18.

$$\texttt{cpine} = \begin{bmatrix} 0 & 20 & 99 & 100 & 120 & 121 & 200 & 250 & 300 & 350 & 400 & 600 & 800 \\ 479 & 479 & 479 & 479 & 479 & 408 & 408 & 398 & 326 & 220 & 163 & 120 & 110 \\ 1530 & 1530 & 1770 & 13600 & 13500 & 2120 & 2000 & 1620 & 710 & 850 & 1000 & 1400 & 1650 \end{bmatrix} \tag{3.18}$$

The model discretises the wooden element into 32 different elements. For finite element analysis, there are always more elements used to generate the model than needed for evaluation. This is done to improve the accuracy of said model. The model is a one-dimensional finite element model that takes time differentiation into account.

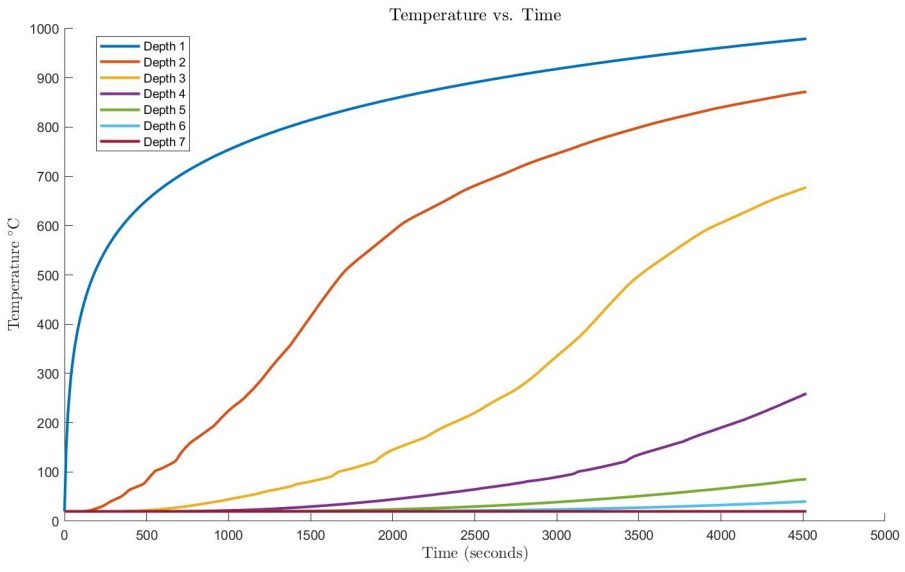

Figure 3.5: Output of finite element model using κ-values as indicated in EN 1995:1-2-2004

3.2.3 Adapted Model

The model was changed into a function that takes κ-values and provides a new temperature distribution over the elements for the different κ-values. This function is used in the posterior calculation to determine the likelihood function.

3.3 Inversion method

The basis of the stochastic analysis is the adapted Bayesian equation 3.19 below. Each aspect of this equation below will be further explored in the sections below.

$$\pi^*(x|T) = \exp\left(-\frac{(\mu - x)^2}{2\sigma_\mu^2}\right) \cdot \exp\left(-\frac{(T - M(x))^2}{2\sigma_{\text{temp}}^2}\right) \tag{3.19}$$

3.3.1 Prior probability

$$\pi(x) = \exp\left(-\frac{(\mu - x)^2}{2\sigma_\mu^2}\right) \tag{3.20}$$

The prior probability function (Equation 3.20) is based on the κ-values assumed prior to any simulation or analysis. The σ_μ in this equation was assumed to be equal to 0.13 W/m·K, In this case, the prior values are indicated as μ and refer to the vector of κ-values(3.21) at specific temperatures as indicated.

$$\mu = \begin{bmatrix} 0.12 \\ 0.12 \\ 0.12 \\ 0.12 \\ 0.15 \\ 0.07 \\ 0.09 \\ 0.35 \\ 1.5 \end{bmatrix} \begin{matrix} 0\ ^\circ\text{C} \\ 60\ ^\circ\text{C} \\ 100\ ^\circ\text{C} \\ 140\ ^\circ\text{C} \\ 200\ ^\circ\text{C} \\ 350\ ^\circ\text{C} \\ 500\ ^\circ\text{C} \\ 800\ ^\circ\text{C} \\ 1200\ ^\circ\text{C} \end{matrix} \tag{3.21}$$

The x (in Equation 3.20) refers to a vector of randomised κ-values that correspond with the same temperatures as the values in the μ vector. The first iteration of randomised κ-values are generated by creating a random perturbation of the μ vector. By multiplying the μ vector with $((0.5 + \text{rand}) \cdot 1.5)$ the first values of x are guaranteed to be within an acceptable range of the

prior values. The process of obtaining the x vector after the first iteration is discussed later in section 3.3.3.

Initially, the program was written to generate completely random new values for the first iteration of x. This later proved to not only be unnecessary but also made the process less accurate as there was a larger burn-in period before the values were anywhere near the actual solution. To increase the accuracy and reduce the number of times the program needed to run to produce a sufficient number of accurate samples, the program was changed to the current method. The prior function in this case was relatively easy to generate and incorporate into the program as a well-defined list of prior values exists.

3.3.2 Likelihood probability function

$$\pi(T) = \exp\left(-\frac{(T - M(x))^2}{2\sigma_{\text{temp}}^2}\right) \tag{3.22}$$

The likelihood probability was more complex to implement, as this required utilisation of the function created from the finite element model as discussed in section 3.2. This function will output the probability of the modelled values $M(x)$ given the measured temperature values (T). As can be seen in Equation 3.22, the $M(x)$ vector is written as a function. The function indicated here takes the new randomised x vector and then runs the model to provide a new temperature distribution over time at various nodes. The output of the finite element model was reduced such that only the nodes at the same depths as the thermocouples are provided to the likelihood function. For the likelihood function, the σ_{temp} value was assumed to be 15°C.

3.3.3 Markov Chain Monte-Carlo integration

The two main parts of the MCMC integration (as mentioned in section 2) are: how a value is deemed acceptable (Monte Carlo), and how the next random sample is selected after a previous sample is accepted (Markov Chain).

As explained in Section 2.4.1 a step size is a crucial part of determining the next random sample. For this project, a step size of 0.05 W/m·K was chosen. Compared to the example shown in Figure 2.1, the actual problem is quite more complex. For this project, a log-normal distribution was chosen instead of a uniform distribution. If every coordinate direction in the aforementioned simple example is seen as a single entry in the x vector, then the example has three κ-values. The problem also technically becomes ten-dimensional, as there are ten separate independent κ-values that must be chained. An important part of the `takesteps.m` (Appendix A) was to ensure the steps are only taken in a logical direction and that they would not move into an illogical or improbable range. Negatives were specifically forbidden, as a negative thermal

diffusivity would mean that heat flows in a direction opposite to the thermal gradient. Provision was made in the function to prevent the algorithm to run away from what we know to be the general area. TODO

The acceptance criterion of the new x-vector is based on the proximity of the new posterior value to the reference posterior value and the previous posterior. //TODO A potential problem encountered with the standard acceptance probability method (shown in Section 2.4.2) is that the magnitudes of the values were not considered. This problem lead to many false positives, as incorrect values were accepted even though they were not acceptable. The acceptance criterion was based on Equation 3.23

$$\exp\left(\frac{\pi^*(x_{n+1}) - \pi^*(x_n)}{\frac{\pi^*(x_{\text{ref}})}{i}}\right) \text{with} \quad i = 50 \tag{3.23}$$

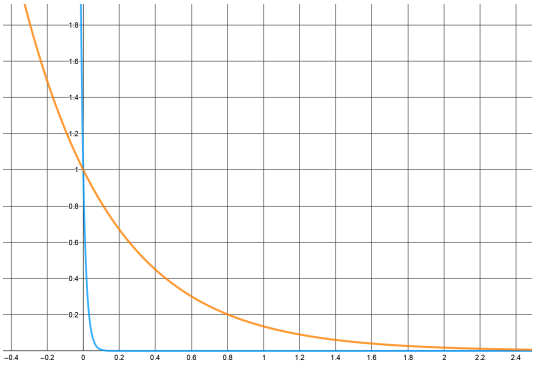

Figure 3.6: Graph explaining the difference in acceptance rates (Generated at https://www.geogebra.org/graphing/g7kyzwce)

3.4 Optimisation to determine MAP

The maximum a posteriori of the posteriori function was also determined to allow for further comparison of results. All the values and constants except for the κ-values were kept the same as in the MCMC integration to allow the results to be compared on the same basis. The optimisation to determine the maximum value of the posteriori function was initially done utilising the built-in Matlab optimisation algorithm `femsearchmin.m`. Since the built-in optimisation intends to minimise the function the probability was multiplied with -1 such that the minimum found is truly the maximum. After initial analysis, the maximum was found at negative κ-values, as previously stated that is illogical and impractical. Further research on various adaptations of the built-in function lead to finding the `femsearchminbnd.m` adaptation by

D'Errico (2021). This was used to limit the search area to only positive κ-values. Further, the algorithm was set to only iterate a thousand times and stop if the points of the simplex are within 0.009 of each other. The start point for the algorithm was chosen to be the κ-values from the EURO code.

A problem that arose was that the function could get stuck at a local maximum. This can be seen in Figure 4.1 on the histogram for 140°C

Chapter 4

Results

The results of running the algorithm until 20 000 acceptable values are found is shown below.)TODO add more.

4.1 Resulting k-values

The thermal conductivity (κ-values) at key temperatures was the main goal of this project. As can be seen in Figure 4.1 there was quite a drastic difference in the thermal diffusivity at 1200 °C and between 0°C and 200°C. thee large difference at 1200°C is due to how our model is created.(TODO?) Most of the energy at that temperature is radiated?(TODO)

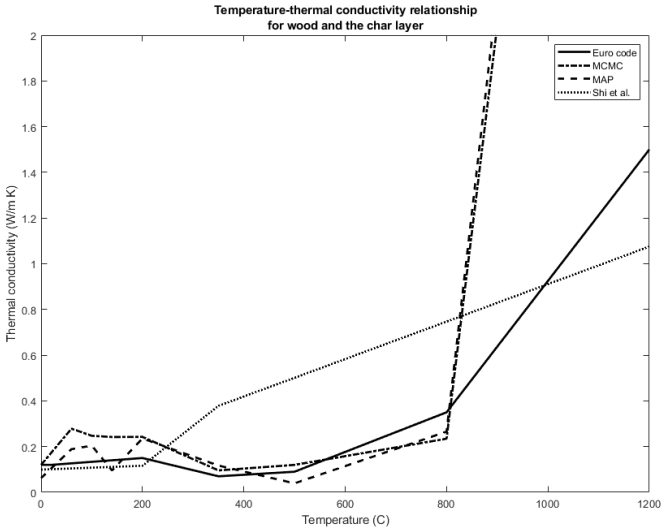

Figure 4.1: Resulting κ values compared to Euro-code standard values

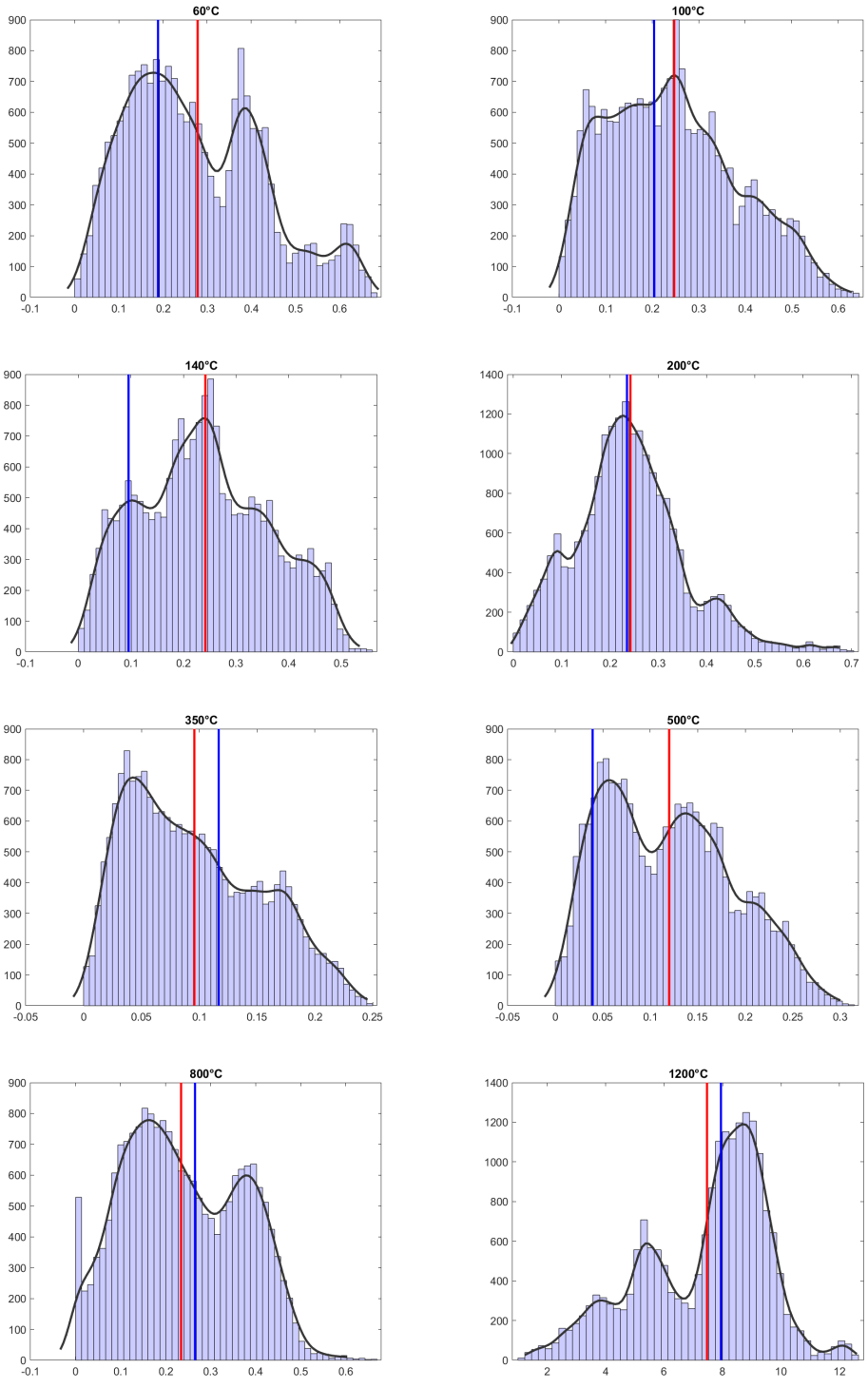

Figure 4.2: Histographs showing distribution at different temperatures

Chapter 5

Discussion

In Figure B the difference in output from running the model with the new κ-values, Euro code κ and the measured data can be seen.

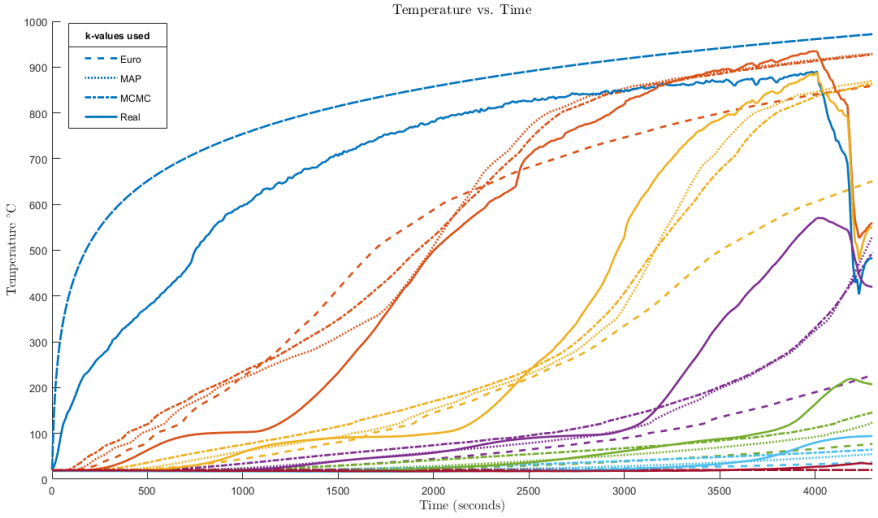

The κ-values obtained from the MAP and MCMC analysis give a more accurate model output than those from the Euro-code. The increased accuracy that the new κ-values provide, serves as a proof of concept that MCMC analysis can be used to determine more accurate fire ratings and specifically fire resistance.

Fire resistance is measured in minutes, this indicates the amount of time from the start of the fire until a specific condition is met. The main conditions taken into account are accounted for by the REI marker system. Where R indicates the load-bearing capacity of the structural element, the associated time indicates when the element can no longer carry the design load. E refers to the integrity of the element and the time indicates how long after ignition

the fire penetrates the element and is visible on the non-heated side. The last is the insulation ability, a limit is set to the temperature of the non-heated side. Time corresponding with that rating refers to when that temperature is exceeded on the non-heated side.

With further development of analytical determination of thermal conductivity and applied finite element models, the data obtained from fire test could be used in a model to determine the REI markers of different size elements.

The accuracy of the Markov Chain Monte-Carlo analysis can be increased by modelling the standard deviation, of both the temperatures and the κ values, as random values and solving for them as well. This would make the analysis more heuristic and decrease the dependence of the results on assumptions made by the researcher. Additionally the program could've been run for a longer time to ensure more samples. and thereby a closer approximation to the population mean.

The MAP analysis could be fine-tuned yet that would be pointless as it is already known that the probability of the thermal conductivity is not symmetrically distributed and that the mean is a more accurate description of the data than the Maximum a posteriori.

In retrospect there should have been more pretreatment? of the measured data before analysis was done. Inaccuracies arose due to the first 90 sec of the measurements being taken before the furnace was turned on and the thermocouples still measuring after the fire died down. These measurement discrepancies between model and measurement should have been better taken into account and excluded form modelling.

This research can be expanded and applied to the measured data available for Eucalyptus. Applying the same algorithm to different data sets and obtaining accurate modelling from both data sets would be confirmation that the algorithm is accurate enough to be further explored for usage in practice. After thorough exploration of the algorithm with the current model, the model can be expanded to a two-dimensional or three-dimensional model.

Chapter 6

Summary and Conclusion

Further development of this concept could lead to simplified methods of calculating the fire rating of specifically SA-Pine as well as other timber samples.

Appendix A

Relevant code segments

Below are the relevant code segments taken from the Matlab code that was used to generate the final samples used for analysis.

Prior function

Determines the probability of x assuming a (NORMAL) probability over the prior values.

```
function q_val = prior_pdf(x_values,sigmaMU)

 global mu_values
 q_val = -0.5*((x_values - mu_values)*(x_values -
    mu_values)')/(sigmaMU^2);

end
```

Likelihood Function

```
function likelihood_pi = likelihood_func(kinput,sigmaT)

% Global variables: physical constants
global_const;
% Global variables: material properties
global_prop
% Global variables: time integration values
global_time;
% Global variables: mesh geometry
global_mesh;
% Global variables of measured temperatures
```

```
global_measuredtemp;

udepths = model_kinput(kinput);
depths_measured = [depth1;depth2;depth3;depth4;depth5;depth6;depth7];
%Where depths measure is the actual measured temperature data from
    the experiment and udepths is the temperature at the same points
    generated by the model using the new k-values.

tempmat = depths_measured - udepths;
likelihood_pi = tempmat(:)'*tempmat(:)/(-2*sigmaT^2);

end
```

Function to take next step

This function takes the current x-vector and generates a new probable x-vector.

```
function xvalue2 = takexsteps(xvalue1)
   global temps mu_values stepsize sigmastepMU sigmastepT

   locsigma = stepsize*mu_values;
   locxvalue = xvalue1 ;;

   lnMu = log(locxvalue.^2 ./ sqrt(locsigma.^2+locxvalue.^2));
   lnSigma = sqrt(log(locsigma.^2./xvalue1.^2 + 1));

   xvalue2 = max(0, lognrnd(lnMu, lnSigma));
   xvalue2(1) = xvalue1(1);

   xvalue2(xvalue2<locsigma/20) =
       (mu_values(xvalue2<locsigma/20)+xvalue2(xvalue2<locsigma/20))/2;

end
```

MAP determination

```
global temps stepsize mu_values
temps = [0,60,100,140, 200,350,500,800,1200];
mu_values = [0.12, 0.12, 0.12, 0.12, 0.15, 0.07, 0.09, 0.35, 1.5];
x_values = mu_values;
stepsize = 0.05;
sigmaT1 = 15;
```

```
sigmaMU1 = 0.13;
instantiate_all();

fminopts = optimset('fminsearch');
fminopts.TolX = 0.0009;
fminopts.MaxFunEvals = 1000;
fminopts.MaxIter = 1000;
lowBound= [0.000, 0.000, 0.000, 0.000, 0.000, 0.0000, 0.0000, 0.00,
    0.1];
upBound = [0.8, 0.8, 0.8, 0.8, 0.8, 0.8, 0.8, 0.8, 20];
%fminopts.AlwaysHonorConstraints =;
% fminopts.PlotFcns = 'optimfplotval';
fun = @(x_values) -1*posteriori_func(x_values,sigmaT1,sigmaMU1);
[mu_map,fval] = fminsearchbnd(fun,
    x_values,lowBound,upBound,fminopts);
```

Appendix B

Detailed results graph

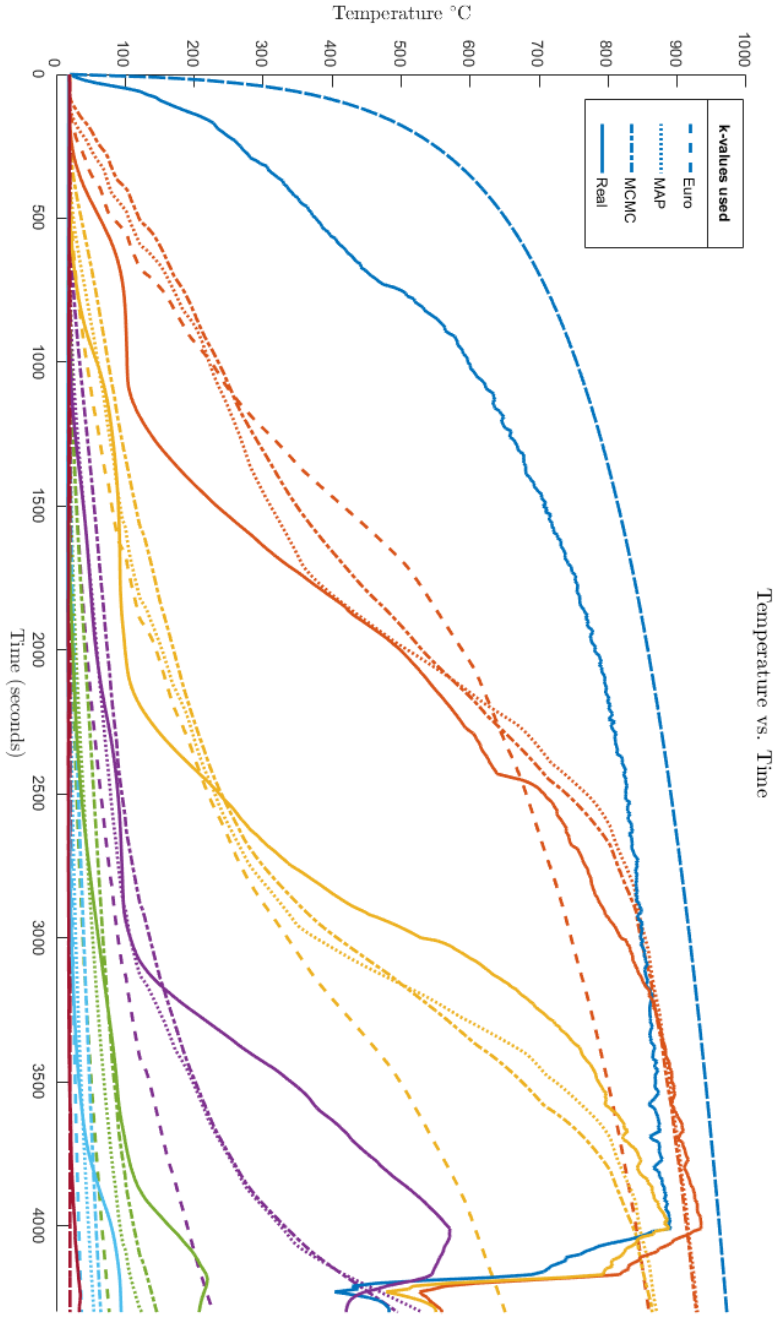

Appendix C

Derivation

$$q_{,x} - f = 0 \ ...(1) \qquad\qquad q = -\kappa u_{,x} \ ...(2) \tag{C.1}$$

Integrating Equation 3.1 (1) over the length of the element(shown in Figure 3.2.1) and introducing a weighting function $w(x)$ we obtain 3.2. Since the derivative of $w(0)$ is known and $q_{,x}$ is unknown. The first term in 3.2 is integrated by parts. After the integration by parts and substituting q with 3.1 (2), Equation 3.3 is created.

$$\int_{x=0}^{L} w q_{,x} dx - \int_{x=0}^{L} w f dx = 0 \tag{C.2}$$

$$\int_{x=0}^{L} w k u_{,x} dx + \int_{x=0}^{L} w f dx - w q|_0^L = 0 \tag{C.3}$$

In Equation 3.3 the u and w need to be defined. Assuming $u \approx u^h$ and $w \approx w^h$ and using the basis function (N^A), Equation 3.4 is obtained.

$$\begin{aligned} u_e^h &= \sum_B N^B d^B \quad ; \quad w_e^h = \sum_A N^A c^A \\ u_{e,x}^h &= \sum_B N_{,x}^B d^B \quad ; \quad w_{e,x}^h = \sum_A N_{,x}^A c^A \end{aligned} \tag{C.4}$$

Substituting the u and w functions back, we obtain the Galerkin weak form shown in Equation 3.5.

$$\begin{aligned} \sum_e \int_{\Omega_e} w_{e,x}^h k u_{e,x}^h dx + \sum_e \int_{\Omega_e} w_e^h f dx - w(L) q_L + w(0) q_0 &= 0 \\ \int_{\Omega_e} \sum_A \sum_B N_{,x}^A c^A k N_{,x}^B d^B dx + \int_{\Omega_e} \sum_A N^A c^A f dx - \sum_{A \in A_N} c^A q^A &= 0 \end{aligned} \tag{C.5}$$

$$\mathbf{c}_e^T \mathbf{K}_e^{AB} \mathbf{d}_e + \mathbf{c}_e^T \mathbf{F}_e^f - \mathbf{c}_e^T \mathbf{F}_e^q \tag{C.6}$$

where

$$K_e^{AB} = \int_{\Omega_e} N_{,x}^A N_{,x}^B k dx$$

$$F_e^{Af} = \int_{\Omega_e} N_{,x}^A f dx$$

$$F_e^{Aq} = \begin{cases} q(x_N) & \text{for } x \in \Gamma_N \\ 0 & \text{for other} \end{cases}$$

$$\begin{aligned} q_{\text{adv}} &= \nu \rho c_p \Delta T \quad = \quad h \Delta T \\ \nu &= \text{velocity m/s} \\ \rho &= \text{density of air} \\ c_\rho &= \text{heat capacity of air} \end{aligned} \tag{C.7}$$

$$\begin{aligned} q_{\text{rad}} &= \varepsilon \sigma \phi \left(T_f^4 - T_S^4 \right) \\ \varepsilon &= \text{emissivity} \\ \sigma &= \text{Stefan-Boltzmann} \\ & \quad 5.670e^{-}8[W/(m^2 K^4)] \\ \phi &= \text{view factor; 1} \quad \text{here} \end{aligned} \tag{C.8}$$

Given that T_S and T_F are known a new equivalent heat flux value can be calculated as in Equation 3.9.

$$q_{\text{con}}^{\text{equiv}} = \kappa^{\text{equiv}} \frac{\Delta T}{\Delta L} = q_{\text{rad}} + q_{\text{adv}} \tag{C.9}$$

Due to the clear relationship between heat flux and thermal diffusivity the equivalent diffusivity(κ^{equiv}) can be calculated as shown below in Equation 3.10.

$$\begin{aligned} \kappa^{\text{equiv}} &= \frac{[q_{\text{rad}} + q_{\text{adv}}]}{\Delta T} \\ &= \frac{\epsilon \sigma \phi \Delta \left(T^4 \right)}{\Delta T / \Delta L} + h \Delta L \\ &= \frac{\epsilon \sigma \Delta \left(T^4 \right)}{\Delta T} + h \end{aligned} \tag{C.10}$$

Diffusion Equation:

$$q_{,x} - f = \frac{\partial Q}{\partial t} = c_\rho \frac{\partial u}{\partial t} \quad ...(1) \qquad q = -\kappa \frac{\partial u}{\partial x} \quad ...(2) \tag{C.11}$$

Substituting Equation 3.11(2) into 3.11 and taking the derivative as indicated ($q_{,x}$) gives Equation 3.12. As previously disccussed heat conduction (α) is heat diffusion (κ) divided by specific heat (c_p).

$$\therefore -\kappa\frac{\partial^2 u}{\partial x^2} - f = c_\rho\frac{\partial u}{\partial t} \rightarrow f = 0 :$$
$$\frac{\partial^2 u}{\partial x^2} = -\frac{c_\rho}{\kappa}\frac{\partial u}{\partial t} \tag{C.12}$$
$$\text{or}$$
$$\frac{\partial u}{\partial t} = -\alpha\frac{\partial^2 u}{\partial x^2}$$

Let $c_p = \lambda$

$$\therefore -\kappa u_{,xx} - \lambda u_{,t} = f \tag{C.13}$$

Then:

$$\int_0^L w q_{,x}\mathrm{d}x - \int_0^L w\lambda u_{,t}\mathrm{d}x - \int_0^L w f\mathrm{d}x = 0 \tag{C.14}$$

Similar to what was done in 3.4 a special approximation is made to obtain Equation 3.15.

$$u \approx u^h \rightarrow u_e^h = \sum_A N^A d^A \quad ; \quad w_e^h = \sum_A N^A L^A \tag{C.15}$$

$$\rightarrow \sum_e \int_{\Omega^e} w_{e,x}^h \kappa u_{e,x}^h \mathrm{d}x_e + \sum_e \int_{\Omega^e} w_e^h \lambda u_{e,t}^h \mathrm{d}x_e + \sum_e \int_{\Omega^e} w_e^h f \mathrm{d}x_e - \sum_{e\in\epsilon_A} w q_N = 0 \tag{C.16}$$

$$*_1 : \int_{\Omega^e} \sum_A \sum_B N_{,x}^A c^A \kappa N_{,x}^B d^B \mathrm{d}x = \sum_A \sum_B \left[\int N_{,x}^A N_{,x}^B \kappa \mathrm{d}x\right] d^B = \mathbf{c}_e^T \boldsymbol{\kappa}_e \mathbf{d}_e$$

$$*_2 : \int_{\Omega_e} \sum_A \sum_B N^A c^A \lambda N^B \dot{d}^B \mathrm{d}x = \sum\sum c^A \left[\int N^A N^B \lambda \mathrm{d}x\right] d^B = \mathbf{c}_e^T \mathbf{M}_e \dot{\mathbf{d}}_e$$

$$*_3 : \int_{\Omega^e} \sum_A N^A c^A f \mathrm{d}x = \sum c \int_B^A N f \mathrm{d}x = \mathbf{c}_e^T \mathbf{F}_e^B$$

$$*_4 : \sum_{A\in\mathcal{A}} \kappa^A q_N^A = \mathbf{c}_e^T \mathbf{F}_e^q$$

From all the above equations the below matrix formulation could be assembled:

$$\mathbf{c}^T \boldsymbol{\kappa}\mathbf{d} + \mathbf{c}^T \mathbf{M}\dot{\mathbf{d}} = \mathbf{c}^T \mathbf{F} \tag{C.17}$$

Solving:(TODO: date 15/10 last)

(1) Set $\mathbf{d}_0 = |---|---|---|$& $\mathbf{v}_0 = \mathbf{0}$Also set α (mixing constant?); Δt (C.18)

(2) Time integration [v-form;Hughes Ch8]$\mathbf{d}_{n+1} = \mathbf{d}_n + (1-\alpha)\Delta\mathbf{v}_n + \alpha\Delta t\mathbf{v}_{n+1}$ (C.19)

$$(\mathbf{M} + \alpha\Delta t\boldsymbol{\kappa})\mathbf{v}_{n+1} = \mathbf{F}_{n+1} - \boldsymbol{\kappa}\tilde{\mathbf{d}}_{n+1} \tag{C.20}$$

if $\mathbf{M}$ and $\boldsymbol{\kappa}$ independent of time and temperature, sufficient to say:

$$\mathbf{v}_{n+1} = (\mathbf{M} + \alpha\Delta t\boldsymbol{\kappa})^{-1}(\mathbf{F}_{n+1} - \boldsymbol{\kappa}\tilde{\mathbf{d}}_{n+1}) \tag{C.21}$$

If κ and λ is independent of position:

$$\begin{aligned}
\kappa_e^{AB} &= \int_0^\ell N_{,x}^A N_{,x}^B \kappa \mathrm{d}x \\
&= \kappa \int_0^\ell N_{,x}^A N_{,x}^B \mathrm{d}x \\
&= \kappa \int_{-1}^{+1} N_{,\xi}^A N_{,\xi}^B \xi_{,x}^2 \, |J| \, d\xi \\
&= \kappa \frac{2}{\ell} \int_{-1}^{+1} N_{,\xi}^A N_{,\xi}^B \mathrm{d}\xi \\
&= \pm\frac{\kappa}{\ell} = \begin{cases} +\frac{1}{2} & \text{if } A = B \\ -\frac{1}{2} & \text{if } A \neq B \end{cases}
\end{aligned} \tag{C.22}$$

$$\therefore \boldsymbol{\kappa}_e = \frac{\kappa}{\ell}\begin{bmatrix} +1 & -1 \\ -1 & +1 \end{bmatrix} \tag{C.23}$$

$$M_e^{AB} = \int_0^\ell N^A N^B \lambda \mathrm{d}x = \lambda \int_0^\ell N^A N^B \mathrm{d}x = \frac{\lambda\ell}{2} \int_{-1}^{+1} N^A N^B \mathrm{d}x \tag{C.24}$$

$$N^1N^1 = \frac{1}{4}(1-\xi)^2; N^2N^2 = \frac{1}{4}(1+\xi)^2; N^1N^2 = \frac{1}{4}(1-\xi^2) \tag{C.25}$$

$$N^1 = \frac{1-\xi}{2}; N^2 = \frac{1+\xi}{2} \tag{C.26}$$

Then

$$\begin{aligned}\int N^1 N^1 &= \frac{1}{4}\left[\xi + \frac{1}{3}\xi^3\right]_{-1}^{+1} = \frac{2}{3}\\ \int N^2 N^2 &= \frac{1}{4}\left[\xi + \frac{1}{3}\xi^3\right]_{-1}^{+1} = \frac{2}{3}\\ \int N^1 N^2 &= \frac{1}{4}\left[\xi - \frac{1}{3}\xi^3\right]_{-1}^{+1} = \frac{1}{3}\end{aligned} \tag{C.27}$$

$$\therefore \mathbf{M}_e = \frac{\lambda\ell}{6}\begin{bmatrix}2 & 1\\ 1 & 2\end{bmatrix} \tag{C.28}$$

$$\mathbf{F}_e^{fA} = \int_0^\ell N f \mathrm{d}x = f\frac{\ell}{2}\int_{-1}^{+1} N \mathrm{d}x = f\frac{\ell}{2} \therefore \mathbf{F}_e^f = \frac{f\ell}{2}\begin{Bmatrix}1\\ 1\end{Bmatrix} \tag{C.29}$$

More generally matrix K_e and M_e are:

$$\begin{aligned}K_e^{AB} &= \int_0^\ell N_{,x}^A N_{,x}^B \kappa \mathrm{d}x \text{ with } \kappa = N^1\kappa^1 + N^2\kappa^2\\ &= \left(\frac{\ell}{2}\right)\left(\frac{\pm 1}{4}\right)\left(\frac{4}{\ell^e}\right)\int_{-1}^{+1}\left[\frac{1-\xi}{2}\kappa^{(1)} + \frac{1+\xi}{2}\kappa^{(2)}\right]\mathrm{d}\xi\end{aligned} \tag{C.30}$$

and

$$M_e^{AB} = \int_0^\ell N^A N^B \lambda \mathrm{d}x \quad \text{with} \quad \lambda = N^1\kappa^{(1)} + N^2\kappa^{(2)} \tag{C.31}$$

If $A = 1$ and $B = 1$ then M_e is calculated as shown below in Equation **??**.

$$\begin{aligned}M_e^{11} &= \left(\frac{\ell}{2}\right)\int_{-1}^{+1}\frac{1}{4}(1-\xi)^2\left[\frac{1-\xi}{2}\cdot\lambda^{(1)} + \frac{1+\xi}{2}\cdot\lambda^{(2)}\right]\mathrm{d}\xi\\ &= \frac{\ell}{16}\int_{-1}^{+1}\left[(1-\xi)^2(1-\xi)\lambda^{(1)} + (1-\xi)^2(1+\xi)\lambda^{(2)}\right]\mathrm{d}\xi\\ &= \frac{\ell}{16}\left[\lambda^{(1)}\int_{-1}^{+1}(1-\xi)^2(1-\xi)\mathrm{d}\xi + \lambda^{(2)}\int_{-1}^{+1}(1-\xi)^2(1+\xi)\mathrm{d}\xi\right]\\ &= \frac{\ell}{16}\left[\lambda^{(1)}\cdot 4 + \lambda^{(2)}\cdot\frac{4}{3}\right]\\ &= \frac{\ell}{4}\left[\lambda^{(1)} + \frac{\lambda^{(2)}}{3}\right]\end{aligned} \tag{C.32}$$

When $A = 2$ and $B = 2$:

$$\begin{aligned} M_e^{22} &= \frac{\ell}{16}\int_{-1}^{+1}\left[(1+\xi)^2(1-\xi)\lambda^{(1)} + (1+\xi)^2(1+\xi)\lambda^{(2)}\right]\mathrm{d}\xi \\ &= \frac{\ell}{4}\left[\frac{\lambda^{(1)}}{3} + \lambda^{(2)}\right] \end{aligned} \tag{C.33}$$

When $A = 1$ and $B = 2$ **or** $A = 2$ and $B = 1$:

$$\begin{aligned} M_e^{12} &= \frac{\ell}{16}\int_{-1}^{+1}\left[(1-\xi^2)(1-\xi)\lambda^{(1)} + (1-\xi^2)(1+\xi)\lambda^{(2)}\right]\mathrm{d}\xi \\ &= \frac{\ell}{4}\left[\frac{\lambda^{(1)}}{3} + \frac{\lambda^{(2)}}{3}\right] \\ &= \frac{\ell}{12}\left[\lambda^{(1)} + \lambda^{(2)}\right] \end{aligned} \tag{C.34}$$

The matrix can then be assembled from the above Equations **??**,**??** and **??**:

$$\begin{aligned} \mathbf{M}_e &= \frac{\ell}{4}\left(\lambda^{(1)}\begin{bmatrix}1 & \frac{1}{3}\\ \frac{1}{3} & \frac{1}{3}\end{bmatrix} + \lambda^{(2)}\begin{bmatrix}\frac{1}{3} & \frac{1}{3}\\ \frac{1}{3} & 1\end{bmatrix}\right) \\ &= \frac{\ell}{12}\left(\lambda^{(1)}\begin{bmatrix}3 & 1\\ 1 & 1\end{bmatrix} + \lambda^{(2)}\begin{bmatrix}1 & 1\\ 1 & 3\end{bmatrix}\right) \end{aligned} \tag{C.35}$$

The same can be done to assemble the K matrix as shown below.

$$\begin{aligned} K_e^{AB} &= \left(\frac{\pm 1}{2\ell}\right)\int_{-1}^{+1}\left[\frac{1-\xi}{2}\kappa^{(1)} + \frac{1+\xi}{2}\kappa^{(2)}\right]\mathrm{d}\xi \\ &= \left(\frac{\pm 1}{2\ell}\right)\left[\kappa^{(1)} + \kappa^{(2)}\right] \end{aligned} \tag{C.36}$$

$$\mathbf{K}_e = \frac{1}{2\ell}\left(\kappa^{(1)}\begin{bmatrix}1 & -1\\ -1 & 1\end{bmatrix} + \kappa^{(2)}\begin{bmatrix}1 & -1\\ -1 & 1\end{bmatrix}\right) \tag{C.37}$$

There after the $\mathbf{F}_e$ matrix

$$\begin{aligned} F_e^A &= \int_0^\ell N^A f\,\mathrm{d}x \\ &= \frac{\ell}{2}\int_{-1}^{+1} N^A f\,\mathrm{d}\xi \end{aligned} \tag{C.38}$$

$$\begin{aligned} F_e^1 &= \frac{\ell}{2}\int_{-1}^{+1}\left(\frac{1-\xi}{2}\right)\cdot\left[\frac{1-\xi}{2}\cdot f^{(1)} + \frac{1+\xi}{2}\cdot f^{(2)}\right] \\ &= \frac{\ell}{8}\int_{-1}^{+1}\left[(1-\xi)^2\cdot f^{(1)} + \left(1-\xi^2\right)\cdot f^{(2)}\right]\mathrm{d}\xi \end{aligned} \tag{C.39}$$

$$F_e^2 = \frac{\ell}{8}\int_{-1}^{+1}\left[(1-\xi^2)\cdot f^{(1)} + (1+\xi)^2\cdot f^{(2)}\right]\mathrm{d}\xi \tag{C.40}$$

$$\begin{aligned}\therefore \mathbf{F}_e &= \frac{\ell}{8}\left(f^{(1)}\begin{Bmatrix}\frac{8}{3}\\ \frac{4}{3}\end{Bmatrix} + f^{(2)}\begin{Bmatrix}\frac{4}{3}\\ \frac{8}{3}\end{Bmatrix}\right) + \sum_{A\in\mathcal{A}_N} q^{(A)}\begin{Bmatrix}-\delta^{A1}\\ +\delta^{A2}\end{Bmatrix}\\ &= \frac{\ell}{6}\left(f^{(1)}\begin{Bmatrix}2\\ 1\end{Bmatrix} + f^{(2)}\begin{Bmatrix}1\\ 2\end{Bmatrix}\right) + \sum_{A\in\mathcal{A}_N} q^{(A)}\begin{Bmatrix}-\delta^{A1}\\ +\delta^{A2}\end{Bmatrix}\end{aligned} \tag{C.41}$$

TODO: uppercase or lowercase A1 and A2 with deltas?

After assembly but before Dirichlet boundaries are applied

$$\bar{\mathbf{c}}^T\bar{\mathbf{K}}\bar{\mathbf{d}} + \bar{\mathbf{c}}^T\bar{\mathbf{M}}\dot{\bar{\mathbf{d}}} = \bar{\mathbf{c}}^T\bar{\mathbf{F}} \tag{C.42}$$

When the Dirichlet boundaries below (Equation **??**) are applied to the matrices shown in Equation **??** , they can be simplified to Equation **??**.

$$\begin{aligned} c_1 = 0 \quad &\text{and} \quad c^{np} = 0\\ d_1 = u_{\text{fire(t)}} \quad &\text{and} \quad d^{np} = u_{\text{air}}\end{aligned} \tag{C.43}$$

Then:

$$\mathbf{c}^T\cdot\mathbf{K}\cdot\mathbf{d} + \mathbf{c}^T\cdot\mathbf{M}\cdot\dot{\mathbf{d}} = \mathbf{c}^T\cdot\mathbf{F}' - \mathbf{c}^T\left(\{K'\}d' + \{K^{np?}\}d^{np?}\right) - \mathbf{c}^T\left(\{M'\}\dot{d}' + \{M^{np?}\}\dot{d}^{np}\right) \tag{C.44}$$

And so:

$$\mathbf{K}\cdot\mathbf{d} + \mathbf{M}\cdot\dot{\mathbf{d}} = \mathbf{F}' - \mathbf{F}^{Ke?} - \mathbf{F}^{Me?} = \mathbf{F} \tag{C.45}$$

Solve as

$$\begin{aligned}\tilde{\mathbf{d}}_{n+1} &= \mathbf{d}_n + (1-\alpha)\Delta t\mathbf{v}_n\\ (\mathbf{M}+\alpha\Delta t\mathbf{K})\mathbf{v}_{n+1} &= \mathbf{F}_{n+1} - \mathbf{K}\tilde{\mathbf{d}}_{n+1}\\ \rightarrow \mathbf{v}_{n+1} &= (\mathbf{M}+\alpha\Delta t\mathbf{K})^{-1}(\mathbf{F}_{n+1} - \mathbf{K}\tilde{\mathbf{d}}_{n+1})\\ \rightarrow \mathbf{d}_{n+1} &= \tilde{\mathbf{d}}_{n+1} + \alpha\Delta t\mathbf{v}_{n+1}\\ \mathbf{v} &= \dot{\mathbf{d}}\end{aligned} \tag{C.46}$$

Appendix D

Program

Date	What should be done before then
4 Jun	Topic allocated. Contact study leader
23 Jun - 31 Jul	Exams and Recess
10 Aug - 23 Aug	Work on Introduction and Literature study for project proposal
24 Aug	Submit project proposal
25 Aug - 2 Sep	Familiarize with FEM model and MCMC process
2 - 10 Sep	Begin coding a basic MCMC process
10 - 17 Sep	Testweek, minimal time can be alloted to skripsie
18 - 30 Sep	Work on MCMC code during recess
1-8 Oct	Finalise Matlab program for MCMC analysis
8-10 Oct	Run simulation
10 - 17 Oct	Add results, discussion of result and conclusion to report
18 Oct	Submit final draft report
20 - 28 Oct	Finalise report and correct as suggested by study leader
28 - 30 Oct	Print and bind report
1 Nov	Submit report

Appendix E

GA outcomes

GA1: Problem Solving

In Chapter 1 the problem as well as the relevant aims and objectives are explained. The problem is approached systematically and a solution is proposed in Chapter 3.

GA2: Application of scientific and engineering knowledge

The problem tackled in this project was mathematically and statistically complex. The report was laid out in a way that would make sense to the reader even if they had minimal understanding of the MCMC algorithm. The limitations of this project were presented in Chapter 5.(TODO)

GA4: Investigations,experiments and data analysis

An overview of the available knowledge and previous studies on the matter is presented in Section 1.3. Multiple versions of the final algorithm were considered, corrected and fine-tuned. The results are analysed and discussed in Chapter 4 and 5. A final conclusion was draw and presented in Chapter 6.

GA5: Engineering methods , skill and tools, including IT

The following subjects were directly relevant and needed for the completion of this project:

- Informatics 244, 314;
- Applied Mathematics 252;
- Engineering Statistics 314;
- Engineering Mathematics 115, 145, 214;

List of References

Brownlee, J. (2019 Nov [Online]). A gentle introduction to markov chain monte carlo for probability. Machine Learning Mastery, Blog.
Available at: https://machinelearningmastery.com/markov-chain-monte-carlo-for-probability/

CEN (2004). *BS EN 1995-1-2:2004. Eurocode 5: Design of timber structures - General - Structural fire design.* BSI, London.

Cheng, A. and Cheng, D. (2005 03). Heritage and early history of the boundary element method. *Engineering Analysis with Boundary Elements*, vol. 29, pp. 268–302.

Cook, J.D. (2016 Jan [Online]). MCMC burn-in. John D. Cook Consulting.
Available at: https://www.johndcook.com/blog/2016/01/25/mcmc-burn-in/comment-page-1/?unapproved=1094214&moderation-hash=912d585bd365341b032df1d4f1bddf3b#comment-1094214

Courant, R. (1943). Variational methods for the solution of problems of equilibrium and vibrations. *Bulletin of the American Mathematical Society*, pp. 1–23. ISSN 1088-9485.
Available at: https://doi.org/10.1090/S0002-9904-1943-07818-4

D'Errico, J. (2021). fminsearchbnd, fminsearchcon. MATLAB Central File Exchange.
Available at: https://www.mathworks.com/matlabcentral/fileexchange/8277-fminsearchbnd-fminsearchcon

Fish, J.J. (2007). *A first course in finite elements*. John Wiley, Chichester. ISBN 9780470035801.

Frayssinhes, R., Girardon, S., Marcon, B., Denaud, L. and Collet, R. (2020). A simple method to determine the diffusivity of green wood. *BioRes*, vol. 3, no. 15, pp. 6539–6549.

Gilks, W.R., Richarson, S. and Spiegelhalter, D.J. (1996). *Markov chain Monte Carlo in practice*. London, 1st edn.

Gupta, K. and Meek, J. (1996). A brief history of the beginning of the finite element method. *International Journal for Numerical Methods in Engineering*, vol. 39, pp. 3761–3774.

ISO (1999). *ISO 834 Fire-resistance test - Elements of building construction*. International Organization for Standardization, Geneva.

Kaipio, J. and Somersalo, E. (2005). *Statistical and Computational Inverse Problems*. Verlag New York.

Lagarias, J., Reeds, J., Wright, M. and Wright, P. (1998 Dec). Convergence properties of the nelder–mead simplex method in low dimensions. *SIAM Journal on Optimization*, vol. 9, pp. 112–147.

Meyn, S. and Tweedie, R. (1993 Jan). *Markov Chains and Stochastic Stability*, vol. 92. Springer Verlag.

Robert, C.P. and Casella, G. (2004). *Monte Carlo Statistical Methods*, vol. 42. 2nd edn. Springer New York. ISBN 9781441919397.

Salvadori, V. (2017 12). *The Development of a Tall Wood Building*. Master's thesis, Polytechnic University of Milan and TU Wien.

Shi, L. and Chew, M.Y.L. (2021 Aug). A review of thermal properties of timber and char at elevated temperatures. *Indoor and Built Environment*, pp. 1–16. https://doi.org/10.1177/1420326X211035557.
Available at: https://doi.org/10.1177/1420326X211035557

van der Westhuyzen, S., Walls, R. and de Koker, N. (2020). Fire tests of south african cross-laminated timber wall panels: Fire ratings, charring rates, and delamination. *Journal of the South African Institution of Civil Engineering*, vol. 62, no. 1, pp. 33–41. ISSN 23098775.

Wagner, P.-R., Marelli, S. and Sudret, B. (2021). Bayesian model inversion using stochastic spectral embedding. *Journal of Computational Physics*, vol. 436, p. 110141. ISSN 0021-9991.
Available at: https://www.sciencedirect.com/science/article/pii/S0021999121000334

White, R. and Dietenberger, M. (2001). Wood products: Thermal degradation and fire. In: Buschow, K.J., Cahn, R.W., Flemings, M.C., Ilschner, B., Kramer, E.J., Mahajan, S. and VeyssiÃ¨re, P. (eds.), *Encyclopedia of Materials: Science and Technology*, pp. 9712–9716. Elsevier, Oxford. ISBN 978-0-08-043152-9.
Available at: https://www.sciencedirect.com/science/article/pii/B0080431526017630

Wiecki, T. (2015 Nov [Online]). MCMC sampling for dummies. While My MCMC Gently Samples, Blog.
Available at: https://twiecki.io/blog/2015/11/10/mcmc-sampling/